ORIGINAL ARTICLE

lajss.org© Latin American Journal of Solids and Structures

www.lajss.org

Prediction Model for Penetration and Cratering of Jetting Projectile Charge into Steel Targets

Dacheng Gao[a], Peng Chen[b], Yiming Li[a], Bihui Hong[a], Wenbin Li[a]*

[a] School of Mechanical Engineering, Nanjing University of Science and Technology, Nanjing 210094, China.
Email: gaodacheng001@163.com, Liyiming0919@163.com, hbh2022@njust.edu.cn, lwb2000cn@njust.edu.cn.
[b] Northwest Industrial Group Co., Ltd., Xi'an 710043, Shanxi, China. Email: cp1212@njust.edu.cn.

* Corresponding author

https://doi.org/10.1590/1679-7825/e9093

Abstract

The radius of jetting projectile charge (JPC) varies significantly from the head to the tail, resulting in the crater formed with a large and uniform radius when penetrating steel target. Current methods for calculating crater radius typically use the average radius without considering JPC radius distribution, leading to large errors in the calculation. Therefore, it is necessary to introduce JPC radius distribution when predicting JPC penetration and cratering. By incorporating the radius distribution in the calculation of JPC break-up time, the modified break-up time model was used to obtain the prediction model for penetration depth. Based on the current jet (JET) cratering theory, JPC radius distribution was introduced to derive the prediction model for crater radius of JPC penetration. The X-ray tests and numerical simulations were used to obtain the radius and velocity distribution of JPC. Finally, the prediction model was verified using data from static penetration tests and literature. The results show that the penetration depth calculated using the modified model had a small error compared to the test results, therefore, the modified model could predict the variation of the crater radius with the penetration depth. And the variation of crater radius was in good agreement with the tests, and accorded with the characteristics of uniform crater radius of JPC penetration. The findings have important guiding significance for JPC design and evaluation.

Keywords

jetting projectile charge, break-up time, penetration, target strength, crater radius

Graphical Abstract

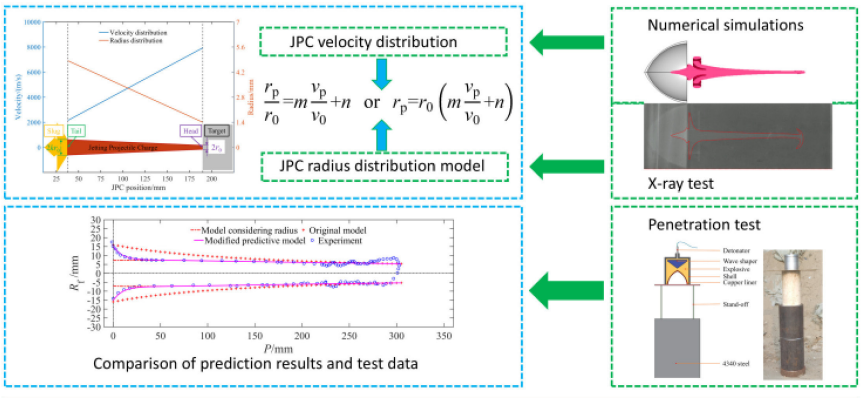

Received April 23, 2026. In revised form May 12, 2026. Accepted May 18, 2026. Available online May 18, 2026.
https://doi.org/10.1590/1679-7825/e9093

1 INTRODUCTION

The K-charge, as disclosed in the patent by Funston et al. (2002), is a compact shaped charge with a small length-to-diameter ratio. It consists of a wave shaper and an eccentric hemispherical liner. The K-charge exhibits high utilization efficiencies of both explosive energy and liner material, and the resulting jetting projectile charge (JPC) combines the advantages of deep penetration depth and large penetration hole diameter. Yang et al. (2016) found through X-ray and static penetration tests that the JPC also features a “uniform crater radius”. This finding directly indicates that the radius distribution along the length direction of the JPC significantly influences its cratering behavior. Therefore, it is an engineering necessity to incorporate the radius distribution into the cratering prediction model for the JPC.

Regarding shaped charges, scholars have conducted extensive research on penetration depth. Traditional penetration theories assumed a constant velocity and density of the jet, whereas an actual jet exhibits a significant velocity gradient along its length (Abrahamson and Goodier 1963). This discrepancy directly affects the accuracy of penetration depth predictions. Considering the velocity distribution of the jet, Allison and Vitali (1963) first proposed the virtual origin model, assuming that the jet velocity decreased linearly along its length and that each jet element maintained a constant velocity during motion (Wang et al. 2018). This model provided an important theoretical framework for subsequent penetration depth predictions, but it did not account for target strength. Elshenawy et al (2018) systematically investigated the effect of target strength on the penetration of shaped charge jets into rolled homogeneous armor (RHA) through experiments and numerical simulations, and found that target strength significantly inhibited penetration depth. Based on this finding, he modified the penetration depth formula proposed by Allison and Vitali by incorporating the analytical method of Wright and Frank (1988) and the target resistance term proposed by Rosenberg and Dekel (1994), thereby improving the prediction accuracy of penetration depth for targets with different strengths. Guo et al. (2023) introduced the jet density distribution on the basis of the virtual origin model and the Szendrei–Held equation, established a penetration depth prediction model for reacting jets, and found that the non-uniform density distribution along the jet length had a significant influence on penetration depth. Zhao et al. (2023) performed numerical simulations of JPC formation and penetration using the LS-DYNA multi-material ALE method, and obtained an optimal match between penetration depth and crater radius. In this study, the radius distribution of the JPC is introduced into the calculation of jet break-up time, and a penetration depth prediction model suitable for the JPC is established, further improving the existing theoretical calculation methods.

Similarly, scholars have investigated the radial response of targets subjected to jet penetration. Among these studies, the work by Szendrei (1983) is representative; he was the first to systematically analyze the cratering behavior during jet penetration and established the fundamental relationship between the cratering velocity and the crater radius. Held and Kozhushko (1999) modified the Szendrei formula and verified the modified formula through experiments, rendering it applicable to a wider range of penetration conditions. Xiao et al. (2010, 2011, 2020) derived the relationship between the cratering velocity and the crater radius, proposed a cratering formula for jet penetration into concrete, and performed numerical calculations and experimental validations. Schwartz (1994) improved upon the SDM model (Simon et al. 1965) and derived a cratering calculation model for jet penetration; the calculated results were in closer agreement with the experimentally obtained cratering profiles, thereby improving the accuracy of cratering predictions. Wang et al. (2008, 2009) proposed the variation law of the jet penetration radius with penetration depth based on Szendrei’s theoretical analysis combined with the virtual origin concept, and her theoretical analysis showed good agreement with the experimental results.

To improve upon the traditional cratering model, recent studies have focused on the influence of non-uniform distribution parameters inside the jet on the radial response of penetration. Guo et al. (2023) introduced the jet density distribution based on the virtual origin model and the Szendrei–Held equation, and established a prediction model for both the penetration depth and the radial cratering of reacting jets. Li and Cheng (2022) derived a cratering equation that accounts for the compressibility of projectile/target materials based on a compressible jet penetration model. Shi et al. (2026) analyzed the roles of shock waves and compressibility during jet penetration into soil, and developed a jet cratering model applicable to soil targets by incorporating the Held cratering model. Furthermore, Xiao et al. (2026) incorporated both the compressibility and the yield strength of the target into a unified computational framework, enabling the penetration resistance to be quantified directly by the material's own compressibility and strength parameters, rather than relying on empirical correlations. Validated by experiments on 45# steel and ultra-high performance concrete, their theoretically predicted crater profiles agreed well with the experimental results. These studies indicate that introducing non-uniform characteristic parameters of the jet, on the basis of the traditional uniform assumption, is an effective approach to improve the accuracy of cratering predictions. Inspired by this, researchers have begun to pay attention to the influence of the jet shape distribution (i.e., the variation of radius along the jet length) on penetration behavior. Fang et al. (2023) established a penetration calculation model considering the jet shape based on the virtual origin hypothesis, and verified the reliability of the model through experiments; however, that study did not yet provide a cratering model that explicitly incorporates the radius distribution.

In current studies on the radial response of steel targets penetrated by JPC, the radius distribution of the JPC has not yet been incorporated into the cratering prediction model. The crater radius calculated using the average radius varies significantly with depth, which is inconsistent with the actual uniform crater radius characteristic of the JPC. This study introduces the JPC radius distribution into the jet break-up time model, obtains a penetration depth prediction model that accounts for the JPC radius distribution, and derives a crater radius prediction model considering the JPC radius distribution based on the cratering theory. To validate the effectiveness of the proposed models, a K-charge was designed and manufactured. The radius distribution of the JPC was obtained by pulsed X-ray, and together with the velocity distribution and the virtual origin position from numerical simulations, the penetration depth and crater radius were predicted. Static penetration tests were conducted for validation. Furthermore, predictions were made and compared with the literature data. The results show that the predictions accounting for the radius distribution are more accurate and agree better with the experiments.

2 PREDICTION MODEL FOR PENETRATION DEPTH AND CRATER RADIUS CONSIDERING JPC RADIUS DISTRIBUTION

2.1 JPC radius distribution model

To accurately describe the radius distribution of the JPC along its length, this study follows the research approach of Fang et al. (2023) regarding the shape distribution characteristics of shaped charge jets. A polynomial function is used to describe the relationship between JPC relative radius and relative position as follows:

$$\frac{r_{\mathrm{p}}}{r_0} = a_{\mathrm{n}} {L_{\mathrm{p}}}^{\mathrm{n}} + \cdots + a_2 {L_{\mathrm{p}}}^2 + a_1 L_{\mathrm{p}} + a_0 \tag{1}$$

where r_{p} represents the radius at different positions of JPC, r_0 is JPC head radius, and L_{p} denotes JPC relative position; a_{n}, ⋯, a_2, a_1, and a_0 are coefficients of the polynomial, which can be obtained by fitting the JPC shape.

The virtual origin model assumes that JPC velocity is distributed linearly along the length, and the relationship between JPC relative velocity and relative position is as follows:

$$\frac{v_{\mathrm{p}}}{v_0} = pL_{\mathrm{p}} + q \tag{2}$$

where v_{p} represents the velocity at different positions of JPC, v_0 is JPC head velocity, L_{p} is the JPC relative position; p and q are coefficients that can be obtained by fitting the JPC velocity distribution.

After further transforming Eq. (2) and substituting it into Eq. (1), the relationship between JPC relative radius and relative jet position can be converted into the relationship between JPC relative radius and relative velocity, which can be expressed as:

$$\frac{r_{\mathrm{p}}}{r_0} = a_{\mathrm{n}} \left(\frac{v_{\mathrm{p}}}{v_0}\right)^n + \cdots + a_2 \left(\frac{v_{\mathrm{p}}}{v_0}\right)^2 + a_1 \left(\frac{v_{\mathrm{p}}}{v_0}\right) + a_0 \tag{3}$$

where a_{n}, ⋯, a_2, a_1, and a_0 are coefficients and can be obtained by fitting JPC profile and velocity distribution data. Where r_{p} represents the radius at different positions of JPC, r_0 is JPC head radius; v_{p} denotes the velocity at different positions of JPC, and v_0 is the JPC head velocity.

A large number of X-ray test results showed that JPC radius is generally linearly distributed along the length direction, as shown in Figure 1.

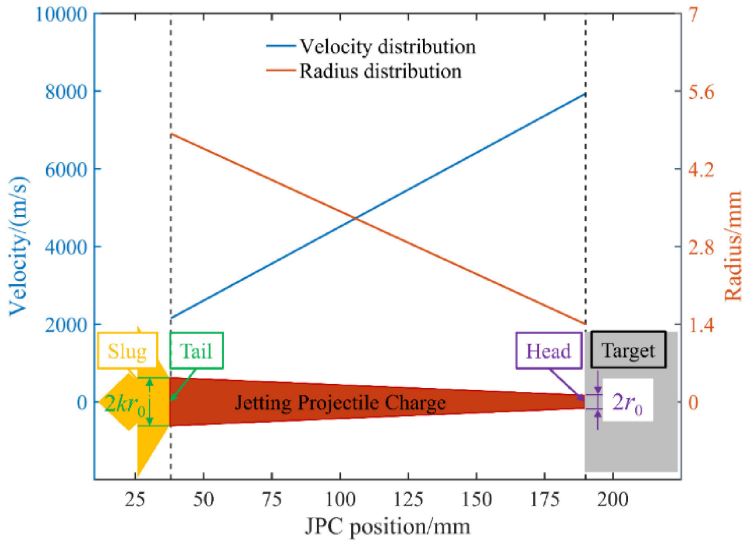

Figure 1 Schematic representation of JPC radius distribution and velocity distribution.

In Figure 1, the head radius is r_0, and the tail radius is k times of the head radius.

The relationship between the relative radius and the relative velocity of JPC can be simplified to a linear relationship, and the relative radius of JPC position is as follows:

$$\frac{r_\mathrm{p}}{r_0}=m\frac{v_\mathrm{p}}{v_0}+n \quad \text{or} \quad r_\mathrm{p}=r_0\left(m\frac{v_\mathrm{p}}{v_0}+n\right) \tag{4}$$

where m and n are coefficients, which can be calculated from the velocity and radius data of JPC head and tail.

2.2 Penetration depth prediction model considering JPC radius distribution

According to the basic assumption of virtual origin proposed by Allison and Vitali (1963), for any time t, the jet penetration depth can be expressed as:

$$P(t)=v_\mathrm{j}(t)t-s \tag{5}$$

where $P(t)$ is the penetration depth, $v_\mathrm{j}(t)$ is the microelement velocity of jet penetrating the target; s is the distance from the virtual origin to the target surface.

When the continuous jet penetrates, Eq. (5) is derived and reintegrated based on Bernoulli equation:

$$v_\mathrm{j}(t)=v_0\left(\frac{t_0}{t}\right)^{\frac{\gamma}{1+\gamma}}=v_0\left(\frac{s}{P+s}\right)^{\gamma} \tag{6}$$

where $\gamma=(\rho_\mathrm{t}/\rho_\mathrm{j})^{0.5}$, ρ_t and ρ_j are the densities of the target plate and the jet respectively; v_0 is the velocity when the jet head impacts the target plate, and t_0 is the moment when the jet head impacts the target plate, that is $v_0t_0=s$.

Substituting Eq. (6) into Eq. (5), the penetration equation can be expressed as:

$$P(t)=s\left[\left(\frac{t_0}{t}\right)^{\frac{\gamma}{1+\gamma}}-1\right]=s\left[\left(\frac{v_0}{v_\mathrm{j}}\right)^{\frac{1}{\gamma}}-1\right] \tag{7}$$

If the penetration ends before the jet breakup, and assuming that the penetration stops at the moment t_c, the cut-off velocity of the final penetration jet is v_c, then the maximum penetration depth of the jet can be obtained, i.e. $P_\mathrm{max}=P(t_\mathrm{c})$.

The use of Eq. (7) is conditioned on the fact that no breakup occurs before the jet penetration is completed. For the penetration of discontinuous jet, Allison and Vitali analyzed test data of shaped charges obtained by BRL (Ballistic Research Laboratories) and concluded that the total penetration depth of the discontinuous jet depends on the total length of all discontinuous particles and is independent of the single particle length of the jet. The penetration depth of the discontinuous jet can be obtained by integrating the penetration velocity:

$$P(t)=\int_{t_0}^{t} U dt=\int_{t_0}^{t_b}\frac{v_j}{1+\gamma}dt+\int_{t_b}^{t}\frac{v_j^{\,2}}{(1+\gamma)v_j(t_b)}dt \ \ if \ \ (t\geq t_b) \tag{8}$$

where t_b is the jet break-up time, $v_j(t_b)$ can be obtained from Eq. (6).

For the break-up time t_b in Eq. (8), Chou and Carleone (1997) established a one-dimensional tensile Lagrangian theoretical model of plastic jet, and detailed the jet growth function and other factors that affect jet stability. In 1992, Chou et al. (1992) proposed a break-up time equation:

$$t_b=w\left(\frac{r_j^2 t}{c_p^2}\right)^{1/3} \tag{9}$$

where the radius r_j and time t of the jet element can be taken at any time before jet breakup. The equation is obtained by fitting based on test data, the coefficient w is 5.0, and $c_p=(\sigma_j/\rho_j)^{0.5}$. For each isotropic jet, σ_j is the yield stress of the jet, for each anisotropic jet, $\sigma_j=(0.5+1/g^2)$, g is the ratio of bending strength to tensile strength.

If JPC radius distribution is not considered in Eq. (9), the calculated break-up time would be a constant value, namely, $r_j^2 t$ remains unchanged for different t values. JPC will stretch longer during the motion, and its radius will also change. Assuming that the JPC density remains constant during the stretching process, according to the mass conservation and the virtual origin theory, the ratio of the radius after stretching to the radius before stretching is $[s/(P+s)]^{0.5}$. Combining Eq. (4), the JPC radius r_j corresponding to penetration depth P is as follows:

$$r_j=r_0\left(\frac{s}{P+s}\right)^{0.5}\left[m\left(\frac{s}{P+s}\right)^{\gamma}+n\right] \tag{10}$$

Substituting Eq. (10) into Eq. (9), the JPC break-up time is as follows:

$$t_b=w\left\{\frac{r_0^{\,2}\left(\frac{s}{P+s}\right)\left[m\left(\frac{s}{P+s}\right)^{\gamma}+n\right]^2 t}{c_p^2}\right\}^{1/3} \tag{11}$$

The SDM model (Simon and Dipersio 1964) provides explicit expressions for penetration depth under three conditions. Breakup is the most common occurrence during JPC penetration process, where Eq. (8) corresponds to case (b).

a. Penetration is completed before JPC breakup.

b. JPC breakup happens during penetration.

$$P_{max}=\frac{(\gamma+1)(v_0 t_b)^{\frac{1}{\gamma+1}}s^{\frac{\gamma}{\gamma+1}}-v_c t_b}{\gamma}-s\ ,\ v_c t_b\left(\frac{v_0}{v_c}\right)^{\frac{1}{\gamma}}\leq s<v_0 t_b \tag{12}$$

c. JPC breakup happens before impacting the target.

Simon and Dipersio (1964) also compared the theoretically calculated penetration depth with test data. In general, good consistency was obtained at a small stand-off (maximum triple the charge diameter); at a large stand-off, the theoretically calculated values were higher than the experimental values (Walters et al. 1988). Eqs. (7) (8) and (12) are the penetration formulas for shaped charge jet of single material represented by copper, and are the penetration formulas of constant density (Wang et al. 2018).

This theory does not consider the effect of target strength, while a large number of studies have found that the yield strength of the target has a significant impact on the penetration depth of the jet. Therefore, Elshenawy and Li investigated the influence of concrete target strength on the penetration of small caliber shaped perforating charge, established a modified term, and introduced it into Eqs. (7), (8), and (12). The modified Eq. (12) is (Elshenawy and Li, 2013, Li and Meng, 2003, Grove et al. 2008):

$$P_{\max}=\left(\frac{(\gamma+1)(v_c t_b)^{\frac{1}{\gamma+1}}\, s^{\frac{\gamma}{\gamma+1}}-v_c t_b}{\gamma}-s\right)\left(1-\lambda\frac{R_t}{\rho_j v_c^2}\right) \tag{13}$$

where λ is the constant determined from experimental data and can be calculated using empirical equations; R_t is the penetration resistance of the target plate, and v_c is the cut-off velocity of the jet penetrating the target plate.

For the penetration resistance R_t of the target plate, Rosenberg and Dekel (1994) discussed the influence of target strength on the penetration depth of long-rod projectiles at different velocities. The yield strengths of the target were 0.5, 1, and 2 GPa. They studied the dependence of target resistance on the strength and density of the penetrator and the target, ignoring the effects of strain rate, strain hardening and temperature softening. The density of the penetrator and the target had little effect on the target resistance, and the target resistance depended on the velocity of the penetrator. They used the spherical cavity expansion model in reference (Wright and Frank 1988) and obtained the penetration resistance R_t of the target. In reference (Elshenawy and Li 2013), the best data were used to fit the cavity expansion model, given by the following equation:

$$R_t=1.38Y_t\left(1+0.5\ln\frac{2E}{3Y_t}\right) \tag{14}$$

where E is Young's modulus and Y_t is the yield strength of the target.

2.3 Crater radius calculation model of JPC penetration considering target strength

Based on reference (Szendrei. 1983, Manfred 1995) and the concept of virtual origin, Wang et al. (2008, 2009) proposed the variation law of the crater radius with jet penetration depth:

$$R_f=r_j\left(\frac{9}{4}+\frac{1}{1+\frac{\sigma}{\rho_t u^2}}\right)^{0.5}\left(1+\frac{1}{4\frac{\sigma}{\rho_t u^2}}\right)^{0.5} \tag{15}$$

Where R_f is the crater radius; σ is the target resistance, i.e., R_t; $r_j=r_0[s/(P+s)]^{0.5}$ represents the corresponding jet radius when the penetration depth is P, r_0 is the jet radius when hitting the target, and generally takes the average jet radius; u is the penetration velocity, and when the target strength is not considered, $u=v_0[s/(P+s)]^{\gamma}/(1+\gamma)$ represents the jet penetration velocity when the penetration depth is P; $\gamma=(\rho_t/\rho_j)^{0.5}$, ρ_t and ρ_j are the densities of the target and the jet respectively; and v_0 is the jet head velocity when hitting the target; s is the distance between the virtual origin and the target. When considering the target strength, u can be calculated by the Alekseevskii-Tate (A-T) equation:

$$u=\frac{v_{\mathrm{j}}-\left[\frac{\rho_{\mathrm{t}}}{\rho_{\mathrm{j}}}v_{\mathrm{j}}^{2}+\left(1-\frac{\rho_{\mathrm{t}}}{\rho_{\mathrm{j}}}\right)\frac{2R_{\mathrm{t}}}{\rho_{\mathrm{j}}}\right]^{0.5}}{1-\frac{\rho_{\mathrm{t}}}{\rho_{\mathrm{j}}}} \tag{16}$$

where v_{j} is the microelement velocity of jet penetrating the target, R_{t} is the target resistance; ρ_{t} and ρ_{j} are the densities of the target and the jet respectively.

Substituting Eq. (10) into Eq. (15), the cratering prediction model considering JPC radius distribution is as follows:

$$R_{\mathrm{f}}=r_0\left(\frac{s}{P+s}\right)^{0.5}\left[m\left(\frac{s}{P+s}\right)^{\gamma}+n\right]\left(\frac{9}{4}+\frac{1}{1+\frac{\sigma}{\rho_{\mathrm{t}}u^{2}}}\right)^{0.5}\left(1+\frac{1}{4\frac{\sigma}{\rho_{\mathrm{t}}u^{2}}}\right)^{0.5} \tag{17}$$

where R_{f} is the crater radius; σ is the target resistance, i.e., R_{t}; r_0 is the jet head radius when hitting the target; $\gamma=(\rho_{\mathrm{t}}/\rho_{\mathrm{j}})^{0.5}$, ρ_{t} and ρ_{j} are the densities of the target and the jet respectively; s is the distance between the virtual origin and the target; P is the penetration depth; m and n are coefficients, which can be calculated from the velocity and radius data of JPC head and tail.

Due to the unloading effect of the target surface, the flow change of the target material was drastic during the cratering stage of JPC penetration. This process was unsteady, and the penetration depth at this stage accounted for a small proportion of the total penetration depth. The corresponding penetration depth was several times the jet diameter (Wang. 2006). For the cratering stage of JPC penetration, the crater radius changed rapidly, which can be modified by the following equation:

$$R_{\mathrm{f}}^{'}=R_{\mathrm{f}}\left(1+fe^{-\frac{P}{2hr_0}}\right) \tag{18}$$

where f is calculated from the crater radius of the target surface, and the penetration depth in the cratering stage is h times the JPC head diameter.

3 PARAMETER ACQUISITION OF PREDICTION MODEL

For the prediction model, it is necessary to obtain some parameters, such as JPC radius distribution and velocity distribution, in order to predict the penetration depth and crater radius. Additionally, it is essential to verify the correctness of the prediction model and compare the differences between the predicted results and the test results. Therefore, numerical simulations, X-ray tests, and penetration tests are required.

3.1 Shaped charge design

Based on the K-charge structure, the shaped charge was designed, which included explosives, shell, wave shaper, and liner. The charge used JH-2 explosives with a diameter and height of 76.0 mm and 84.0 mm, respectively; the liner was made of T2 purple copper with a diameter and height of 69.0 mm and 46.8 mm, respectively; the aluminum alloy shell was used with the wall thickness of 3.5 mm.

3.2 Numerical simulations of JPC formation

3.2.1 Numerical model

JPC formation was a large deformation process, so the arbitrary Lagrange-Eulerian (ALE) algorithm of LS-DYNA was used for numerical simulation. The K-charge was axisymmetric, and the quarter model was used for numerical simulation to reduce calculation time, the numerical simulation model was shown in Figure 2. The detonation mode was the single point detonation at the top center. A non-reflective boundary was imposed on the air to simulate the infinite air domain.

In addition, because the numerical simulation included wave shaper, it was necessary to use *CONTROL_EXPLOSIVE_SHADOW to achieve the diffraction of detonation waves.

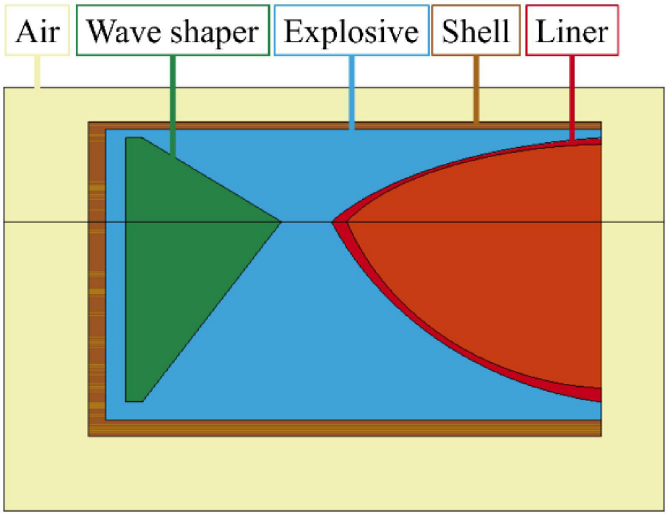

Figure 2 The quarter model for numerical calculation of shaped charge.

3.2.2 Material models

Material models and parameters used in JPC formation simulation in this study are briefly described in this section.

JH-2 explosive was pressed at a pressure of 270MPa for 20 seconds to obtain the shaped charge containing a liner. The charge density was 1.690 g/cm^3, the detonation velocity was 8425 m/s, and the Chapman-Jouguet (C-J) pressure was 29.5 GPa. The equation of state (EOS) of high explosives is the Jones-Wilkins-Lee (JWL) equation (Baudin et al. 2010), and the pressure is expressed as:

$$p_{\mathrm{E}} = A_1\left(1-\frac{\omega}{R_1V}\right)e^{-R_1V} + B_1\left(1-\frac{\omega}{R_2V}\right)e^{-R_2V} + \frac{\omega E_0}{V} \tag{19}$$

where p_{E} is the pressure, V=1/ρ is the relative volume, ρ is the explosive density; A_1, B_1, R_1, R_2 and ω are constants; E_0 is the specific internal energy per unit mass of the explosive. Detailed parameters of JH-2 are shown in Table 1.

Table 1 Parameters related to JH-2 (Hong et al. 2024).

ρ (kg/m^3)	D (m/s)	$P_{\mathrm{C\text{-}J}}$ (GPa)	A_1 (GPa)	B_1 (GPa)	R_1	R_2	ω	E_0 (GPa)
1690	8425	29.5	8.524	0.18	4.6	1.3	0.38	6.04×106

The liner was obtained by turning and processing T2 copper rod material, and the numerical simulation was described by Johnson-Cook (J-C) strength model. The J-C model represents the strength behavior of typical metals under large strains, high strain rate, and high temperature. The model comprehensively takes into account strain strengthening effect, strain rate effect and temperature effect (Song et al. 2019). The J-C constitutive model is defined as:

$$\sigma_{\mathrm{JC}} = \left(A_2 + B_2\varepsilon_{\mathrm{p}}^{N}\right)\left[1 + C\ln\left(\frac{\dot{\varepsilon}}{\dot{\varepsilon}_0}\right)\right]\left[1-\left(\frac{T-T_0}{T_{\mathrm{M}}-T_0}\right)^{M}\right] \tag{20}$$

where A_2, B_2, C, N and M are parameters obtained by fitting; ε_{p} is the effective plastic strain; $\dot{\varepsilon}$ and $\dot{\varepsilon}_0$ are the equivalent plastic strain and reference strain rate, respectively; T, T_0 and T_{M} are the ambient temperature, room temperature, and material melting-point temperature, respectively (Wang et al. 2019).

In addition, Gruneisen's equation of state is used to describe the state of materials at high strain rates, which defines the pressure in the compressed state of the material as:

$$p_{\mathrm{G}}=\frac{\rho_0 c_0^2 \mu\left[1+\left(1-\frac{\gamma_0}{2}\right)\mu-\frac{a}{2}\mu^2\right]}{1-\left(s_1-1\right)\mu-s_2\frac{\mu^2}{\mu+1}-s_3\frac{\mu^3}{\left(\mu+1\right)^2}}+\left(\gamma_0+a\mu\right)E_{\mathrm{G}} \tag{21}$$

The pressure in the expanded state of the material is defined as:

$$p_{\mathrm{G}}=\rho_0 c_0^2\mu+\left(\gamma_0+a\mu\right)E_{\mathrm{G}} \tag{22}$$

where c_0 is the intercept of v_s-v_p curve, s_1, s_2 and s_3 are coefficients of the slope of v_s-v_p curve, v_s and v_p are the impact velocity and particle velocity respectively; γ_0 is the Gruneisen coefficient, and a is the first-order correction of γ_0; $\mu=\rho/\rho_0-1$, ρ and ρ_0 are the density and initial density of the material respectively; E_{G} represents the internal energy.- Table 2 lists the parameters of T2 copper and aluminum.

Table 2 Material parameters of T2 copper and aluminum (Ge et al. 2023).

Material	ρ (kg/m^3)	A_2 (MPa)	B_2 (MPa)	N	C	M	T_M(K)	c_0(m/s)	s_1
Cooper	8960	90	292	0.31	0.025	1.09	1360	3940	1.49
Aluminum	2780	265	426	0.34	0.015	1.00	776	5286	1.40

Some materials used in the numerical simulation, such as phenolic resin and air, are no longer introduced in detail.

3.3 X-ray test design

The X-ray test setup is shown in Figure 3, which includes two X-ray tubes, the shaped charge, the PVC pipe, two film holders, and four pieces of film. The shaped charge was placed vertically on the PVC pipe, and its position along with the PVC pipe was adjusted to align with the intersection axis of the two X-ray tubes. The test determined the light-out time of the X-ray machine and the placement height of the shaped charge through numerical simulation results to ensure that the JPC formation process could be completely presented on the film. One test could obtain two X-ray photos at different moments. After the detonation of the charge, air ionization caused the wires to conduct, serving as the trigger signal for the X-ray machine.

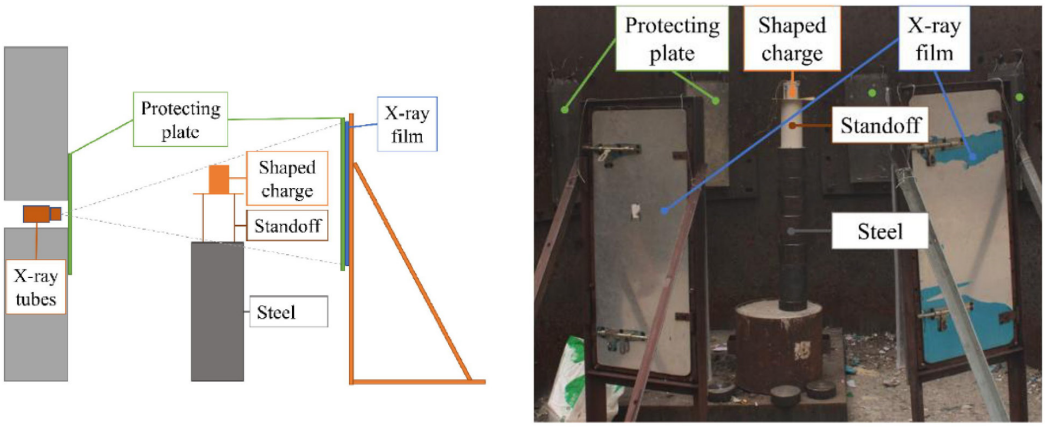

Figure 3 Schematic diagram and setup of X-ray test of JPC formation.

The X-ray films after the test were scanned into pictures, and the pictures were processed by software to make the JPC more clearly visible.

3.4 Test design of JPC penetration into steel target

The test setup is shown in Figure 4. During the test, the PVC tube was placed on an AISI 4340 steel target, and the stand-off was set to 190 mm. The steel target used for the test was AISI 4340 steel with a diameter of 150 mm and a height of 200 mm, and its strength was 892 Mpa. After the test, the steel target was cut open, and the change of crater radius with penetration depth was obtained by software processing.

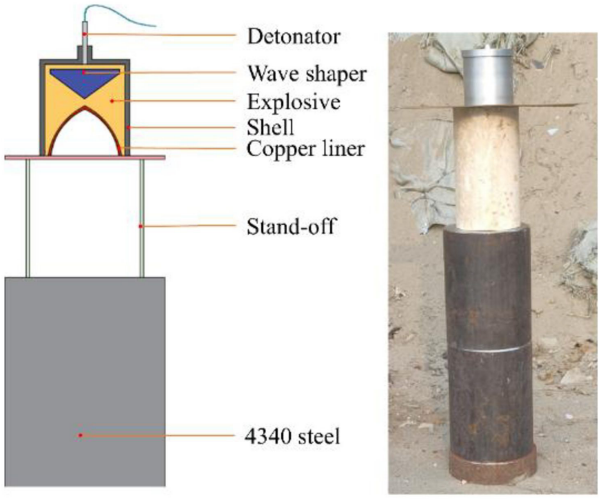

Figure 4 Schematic diagram and setup of JPC penetration into steel target.

3.5 Results and acquisition of input parameters

This section presents the results of numerical simulations, X-ray tests, and penetration tests. Then, the test results are extracted and processed to obtain the input parameters required for the prediction model.

A total of two X-ray tests were conducted. In the first X-ray test, the preset shooting times were 25 μs and 35 μs, capturing only a small portion of JPC, but JPC head velocity could be measured. Before the second test, the height of the charge placement was adjusted, and the shooting times were reset to 30 μs and 40 μs. However, due to the device malfunction, the 40 μs shooting time was not captured, and only the 30 μs shooting time was recorded, and the complete morphology of JPC was captured. After processing, as shown in Figure 5.

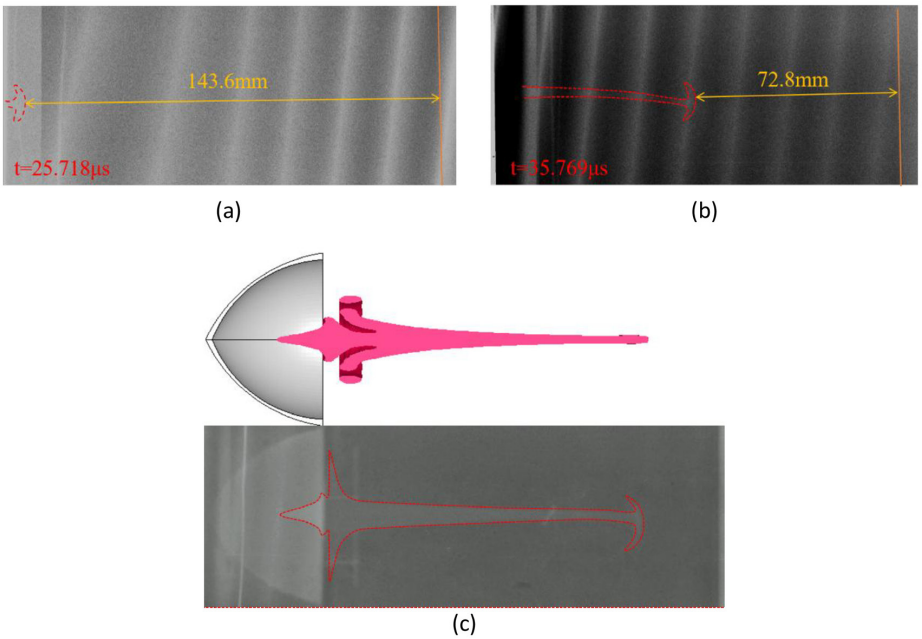

Figure 5 X-ray test results of JPC formation: (a) *t*=25.718 μs, (b) *t*=35.769 μs and (c) comparison of numerical simulation and X-ray test results (*t*=30.884 μs).

The test result for the JPC head velocity, calculated based on Figure 5(a) and 5(b), is 7044 m/s, and the numerical calculation result is 7651 m/s, with an error of 8.61%. The numerical simulation results are consistent with the test results, and the formation process is relatively consistent, which provides effective jet velocity distribution information and provides a basis for the later theoretical calculations. Figure 5(c) shows that JPC radius formed by the charge structure gradually increased from head to tail, showing a linear relationship.

Combining the results from numerical simulations and X-ray tests, the velocity distribution, radius distribution, and the position of virtual origin of JPC can be obtained. The velocity distribution obtained by numerical simulation of JPC formation is shown in Figure 6. The time is four moments before the JPC head impacts the steel target, and L represents the distance from the JPC microelement to the bottom of the liner. The position of virtual origin at each moment can be obtained by the least squares method, and the average value (s=207.9 mm) is obtained at four moments. By this method, the s value of JPC penetrating the target can be obtained.

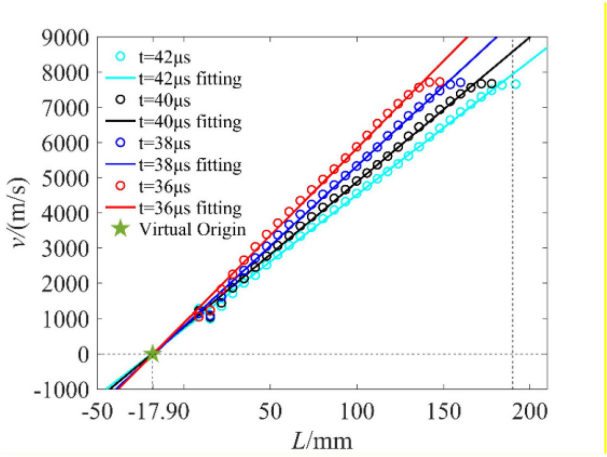

Figure 6 JPC velocity distribution and position of virtual origin.

Two JPC penetration tests into steel target were conducted. Both tests were performed at 2.5 times the standoff distance (s=207.9mm). After the two tests, the crater radius variation law of the steel plate remained consistent, but there was a certain difference in penetration depth. In the later stages of penetration, the JPC broke up into particles, which introduced many uncertainties and affected the penetration, resulting in differences in the penetration results. The cross sections of steel target after the penetration tests are shown in Figure 7:

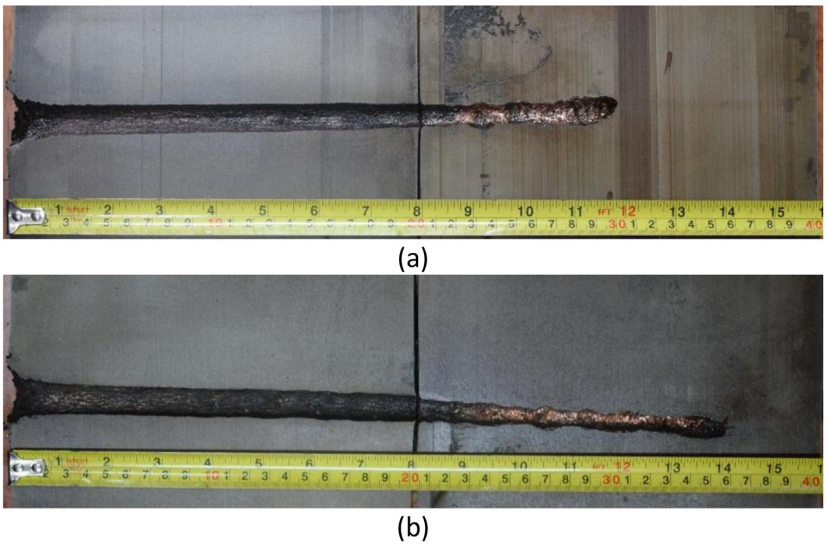

(a)

(b)

Figure 7 Cross sections of the crater formed after JPC penetration into the steel target under 2.5 times the stand-off (s=207.9mm): (a) penetration test 1 and (b) penetration test 2.

To obtain the variation law of the penetration crater with penetration depth, the cross-sectional image shown in Figure 7 was imported into image processing software. First, a coordinate system was established on the image and dimensional calibration was performed to determine the conversion relationship between pixels and actual physical dimensions. Then, the complete contour of the crater in the steel target was manually extracted. Finally, a number of measurement positions were selected along the crater depth direction, and the crater radius at each position was measured sequentially, thereby obtaining the variation curve of the crater radius with penetration depth. For the penetration depth, since the initial conditions of the two tests were identical, the average value of the two was taken as the final result.

In this section, the input parameters for the prediction model were obtained through X-ray tests and numerical simulations, including the velocity v0 and radius r0 of the JPC head, the radius ratio k between the tail and the head of the JPC, and the virtual origin position. In the following, the penetration process of the JPC into a steel target will be predicted and discussed.

4 RESULT AND DISCUSSION

To further verify the accuracy of prediction model, in addition to conducting penetration tests, data from other scholars' literature was also referenced. This included the velocity distribution obtained from numerical simulations, the radius distribution obtained from X-ray tests, and the penetration depth and crater radius obtained from penetration tests.

X-ray tests were used to investigate the formation law of shaped charge with eccentric sub-hemispherical liner of variable wall thickness and with wave shaper in reference (Chen. 2015). The JPC formation shape and parameters such as velocity, length, and diameter were obtained, which verified the validity of numerical simulation. In addition, penetration tests under a small stand-off were carried out, and the variation law of the crater shape with penetration depth at twice the stand-off was obtained. Numerical simulation and X-ray tests were used to study the formation shape of conical shaped charge (CSC), and jet formation parameters such as velocity, length, and diameter were obtained in references (Xu et al. 2019). In addition, jet penetration tests under two kinds of stand-off were carried out, and the variation law of crater radius with penetration depth at two kinds of stand-off was obtained.

4.1 Penetration depth of JPC into steel target

When JPC penetrated continuously, the penetration time t at different penetration depths P was obtained from Eq. (7), and the t-P curve could be drawn; since the radius distribution was considered, the JPC break-up time t_b was not a fixed value, but varied with the change of radius. Combining Eq. (11) with Eq. (7), the corresponding JPC break-up time t_b at different penetration depths P was derived. The t-P curve and t_b-P curve under various conditions in penetration test and in references (Chen. 2015, Xu et al. 2019) are plotted as shown in Figure 8. The red curve in the figure is the t_b-P curve of JPC breakup, and the green curve is the t-P curve of JPC continuous penetration. When P is a constant, if $t<t_{b1}$, it means that no breakup occurs when JPC penetrates; when $t=t_{b1}$, it means that JPC penetrated until breakup occurs at this time; when $t>t_{b1}$, it means that JPC is in the penetration stage of breakup, as shown by the curve composed of black circles in Figure 8. The penetration depth of continuous penetration stage is P_{tb}, and the total penetration depth P_m calculated from Eq. (14) is the P value corresponding to the blue straight line in Figure 8.

Generally, the crater walls formed by penetration and cratering before JPC breakup are relatively smooth and the crater radius changes smoothly. After breakup, JPC particles need repeated cratering, so the crater walls are relatively rough and the crater radius fluctuates greatly. For the test results, the length of the smooth part of crater radius was measured as the penetration depth P_{tb} during JPC continuous penetration stage. The comparison between the calculation results and the test results of penetration depth is shown in Table 3:

The error between theoretical calculation results and test results is within 15%, indicating that the modified prediction model can accurately predict the penetration depth.

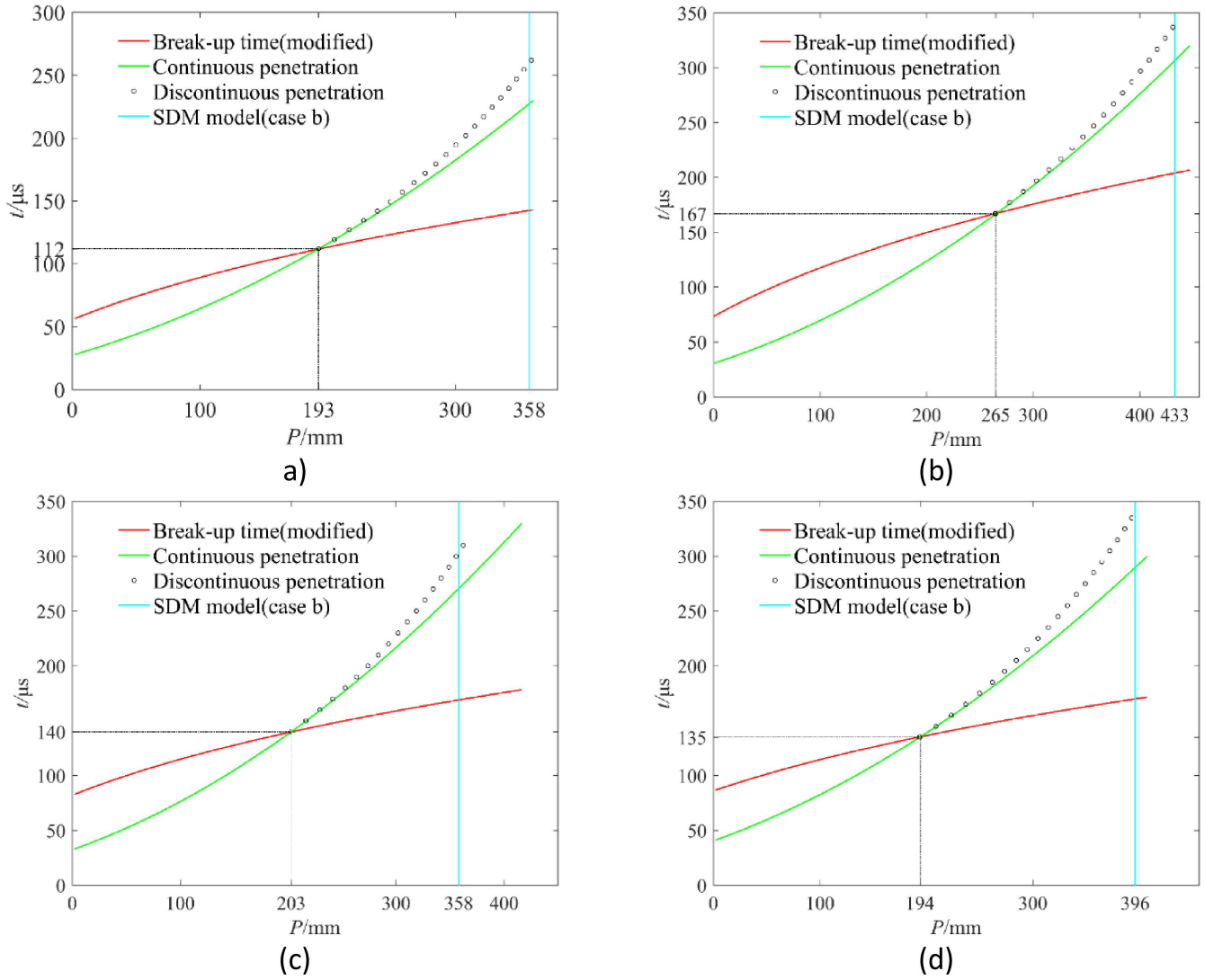

Figure 8 The relationship between penetration time t and penetration depth P: (a) penetration test under 2.5 times the stand-off, (b) test under 3.0 times the stand-off in reference (Chen. 2015), (c) test under 2.0 times the stand-off in references (Chen. 2015) and (d) test under 2.5 times the stand-off in references (Xu et al. 2019).

Table 3 Theoretical calculation results of penetration depth.

Results	Continuous penetration depth P_{tb}			Total penetration depth P_m		
	Test (mm)	Prediction (mm)	Error (%)	Test (mm)	Prediction (mm)	Error (%)
Penetration tests	216	193	-10.6	330	358	8.5
Tests (Chen. 2015)	249	265	6.4	410	433	5.6
Tests (Chen. 2015)	200	203	1.5	382	358	-6.3
Tests (Xu et al. 2019)	210	194	7.6	386	396	2.6

4.2 Crater radius of JPC penetration into steel target

The modified curve of crater radius changing with penetration depth was plotted and compared with the original theory and test data. The results are shown in Figure 9.

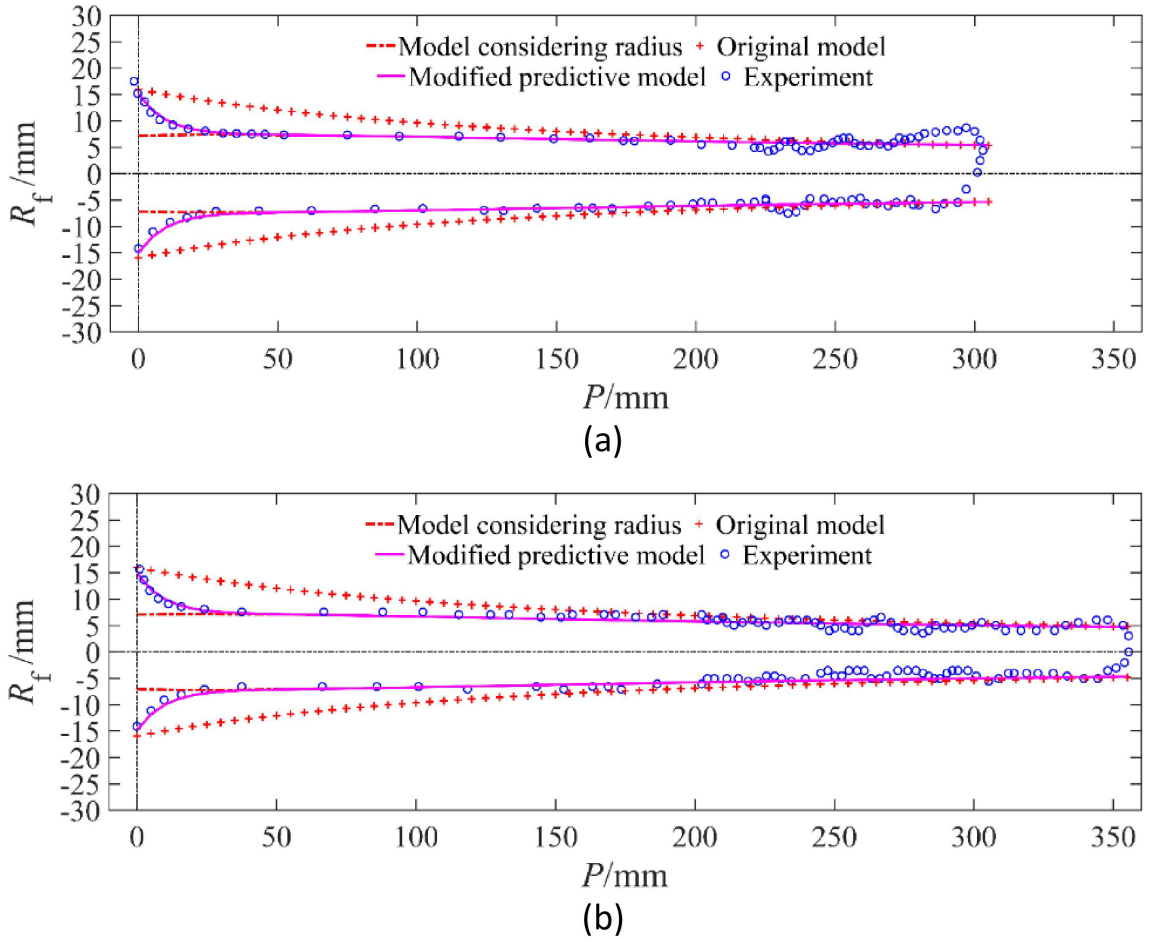

Figure 9 Comparison of prediction results and test data (r_0=1.4 mm, k=3.45, s=207.9 mm): (a) Penetration test 1 under 2.5 times the stand-off and (b) Penetration test 2 under 2.5 times the stand-off

The radius distribution was introduced to predict the crater radius by the JPC parameters in reference (Chen. 2015), which was compared with the test results in reference, as shown in Figure 10.

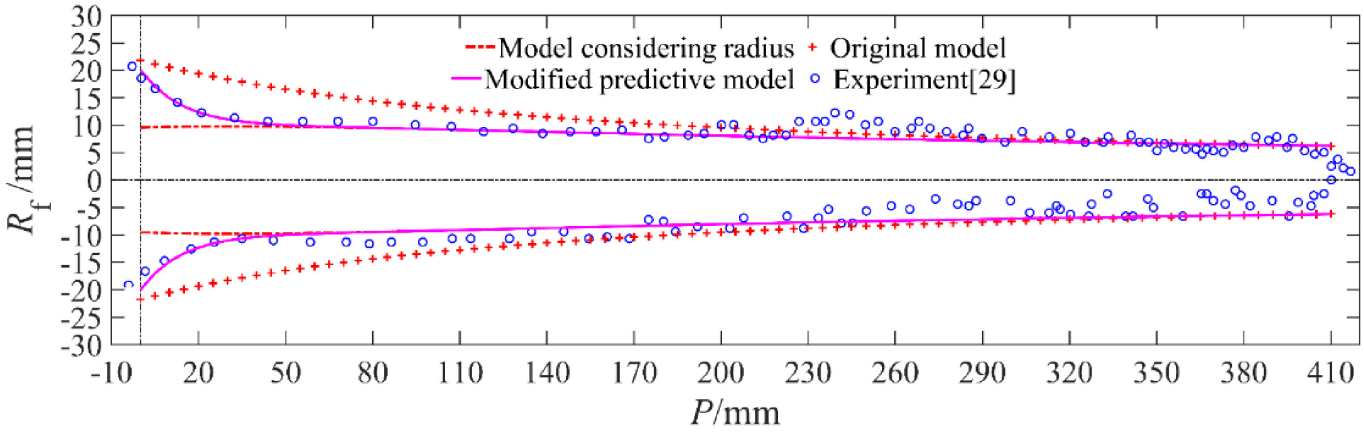

Figure 10 Comparison of crater radius in prediction results and in reference (Chen. 2015) (r_0=2.0 mm, k=3.5, s=209.0 mm).

The radius distribution was introduced to predict the crater radius by the jet parameters in references (Xu et al. 2019), which was compared with the test results in reference, as shown in Figure 11.

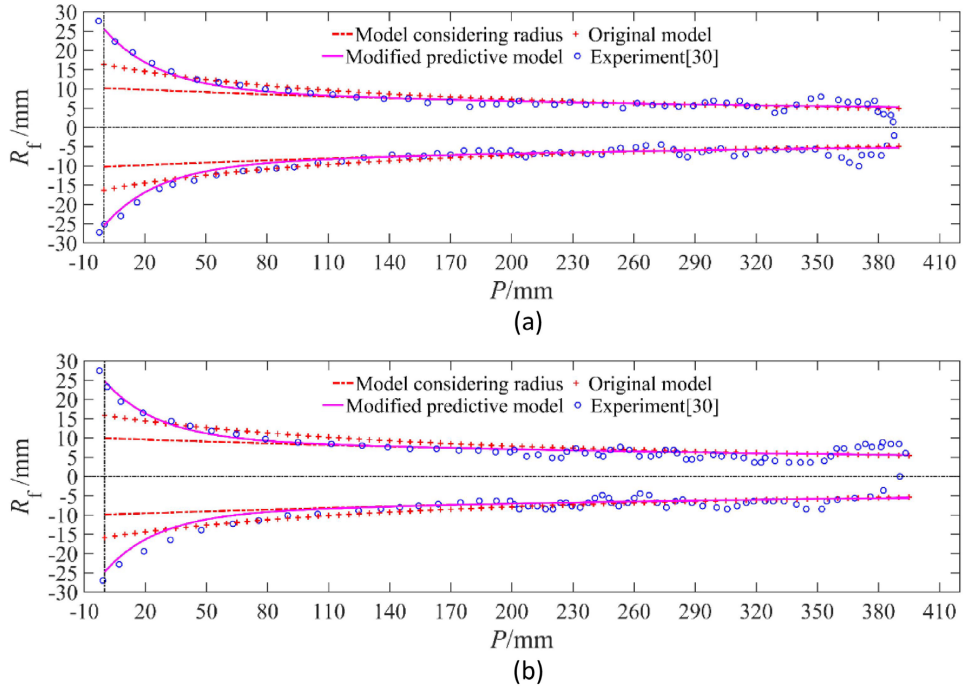

Figure 11 Comparison of crater radius in prediction results and in references (Xu et al. 2019): (a) 2.0 times the stand-off (r_0=2.31mm, k=2.2, s=206.8mm) and (b) 2.5 times the stand-off (r_0=2.22 mm, k=2.2, s=258.3 mm).

It can be seen from Figure 11 that the change of modified crater radius is closer to the test data, and there are only large errors in the later stage of penetration. In the later stage of penetration, the jet breaks up into particles, and the particles need repeated cratering, and there is overturning and lateral motion, which will lead to uneven crater radius formed in the later stage of penetration and difficult to accurately predict.

4.3 Discussion on the ratio *k* of JPC tail radius to head radius

This section discusses the process of radius variation with penetration depth when JPC penetrates steel target under different values of k, as well as the variation law of the final crater radius, and studies the effect of the k value on cratering.

Suppose that the JPC head velocity is v_0, the head radius is r_0, the tail velocity is v_t, and the tail radius is k times of the head, then $m=(k-1)/(v_t/v_0-1)$, $n=1-m$; the average radius $\bar{r}$ is $r_0(k+1)/2$, and JPC radius corresponding to the penetration depth P is $r_j/r_0=[s/(P+s)]^{0.5}$. Take k values from 1.0 to 4.0, and use Eq. (10) to calculate the JPC relative radius r_j/r_0 corresponding to different penetration depths under different k values; at the same time, the JPC relative radius r_j/r_0 corresponding to different penetration depths at different k values is calculated by the average radius. The results are as shown in Figure 12:

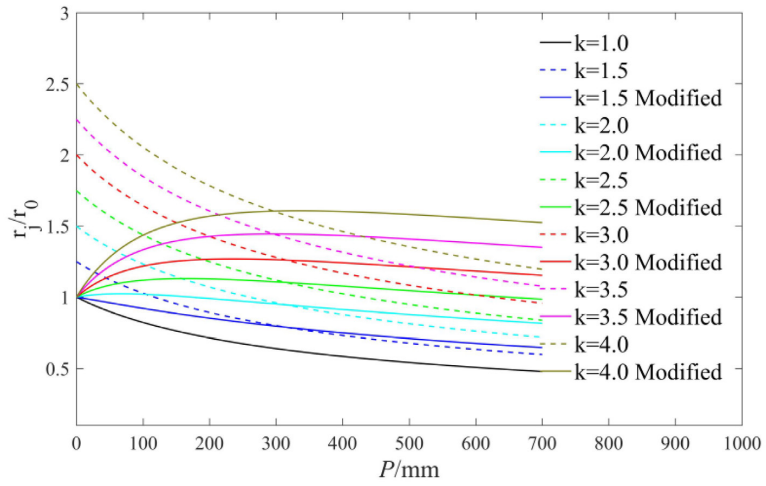

Figure 12 Comparison of JPC relative radius changing with penetration depth at different k values under two radius processing methods.

In Figure 12, when k is not 1, there is an intersection between the radius of linear distribution and the average radius, and the P values corresponding to the intersection are very close; in addition, it can be seen from Eq. (17) that the P values corresponding to the intersection increase with the increase of s. The difference between the radius of linear distribution and the average radius first decreases and then increases with the increase of P, and the difference also increases with the increase of k value. When k≥2, the relative radius of the linear distribution will first increase and then decrease with the increase of P. The JPC penetration velocity will become lower and lower, and the cratering capability will also decrease accordingly. However, because the JPC radius curve has a rising stage first, this will cause the crater radius to increase first and then decrease. As the k value becomes larger, the penetration depth corresponding to the maximum value of the JPC radius curve becomes larger, and the descending section of the radius curve becomes smoother, which makes the crater radius formed by penetration decrease more slowly.

The parameters for JPC penetrating the target are defined as follows: the head velocity v_0 is 7000 m/s, the tail velocity v_t is 2000 m/s, the radius r_0 when the jet head contacts the target is 1 mm, and the distance between the virtual origin and the target is s=250 mm. Take the constant value σ, and use Eq. (14) to calculate R_t. Taking different k values, the R_f predicted by the two radius processing methods are shown in Figure 13.

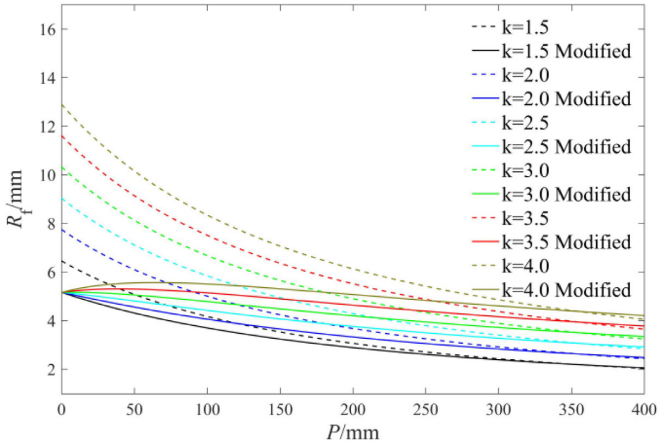

Figure 13 Comparison of crater radius changing with penetration depth at different k values under two radius processing methods.

It can be seen from Figure 13 that as the k value increases, the crater radius formed by penetration decreases slowly, and is more uniform.

5 CONCLUSIONS

In this study, based on the existing theoretical model, the modified prediction equation for penetration and cratering was obtained by introducing JPC radius distribution. X-ray tests were used to verify the effectiveness of the numerical simulation. Combined with the results of numerical simulation and X-ray tests, the penetration depth and the variation of crater radius were predicted. Finally, penetration tests were carried out and compared with the prediction results, moreover, the prediction model was further verified by the literature data, and the following conclusions are drawn:

1. By comparison of numerical simulation and X-ray test results, LS-DYNA can more accurately simulate JPC formation.
2. The continuous penetration depth and final penetration depth of JPC can be obtained from the penetration test results. The results of the modified penetration depth prediction model are close to the test results, indicating that the JPC break-up time calculation model considering the radius distribution is accurate.
3. The results of the two penetration tests show that the crater radius is similar and the variation of crater radius with penetration depth is relatively consistent, which accords with the characteristics of uniform crater radius of JPC penetration. After introducing JPC radius distribution, the variation of crater radius with penetration depth predicted by the penetrating and cratering equation is closer to the test results.
4. For JPC, the ratio k of tail radius to head radius is usually greater than 3. The cratering prediction results considering radius distribution show significant differences compared to using average radius, which can more accurately predict the variation law of crater radius with penetration depth. When the k value is relatively small, such as for JET, the difference of the predicted crater radius results using average radius and considering radius distribution is very small.

The modified cratering prediction model is relatively accurate for JPC (formed by copper liners) penetrating steel targets. No extended research has been carried out for liners and targets of other materials. More test data can further verify the universality of the prediction model. In addition, it is only one of the common cases that the JPC or the jet radius is linearly distributed along the length direction. The relationship between relative radius and relative velocity can be described by polynomial function, which can be applied to more JPC shapes, and the variation of crater radius with the penetration depth can be predicted more exactly.

Acknowledgments

The work presented in this paper was funded by the China Postdoctoral Science Foundation (Grant No. 2022M721614).

Author's Contribuitions: Conceptualization, Dacheng Gao; Methodology, Peng Chen.; Investigation, Bihui Hong; Writing - original draft, Dacheng Gao; Writing - review & editing, Dacheng Gao and Wenbin Li; Funding acquisition, Yiming Li; Supervision, Peng Chen

Data availability statement: Research data is only available upon request

Editor: Marcílio Alves

References

Abrahamson G.R., Goodier J.N. (1963). Penetration by Shaped Charge Jets of Nonuniform Velocity. Journal of Applied Physics 34(1):195-199.

Allison F.E., Vitali R. (1963). A new method of computing penetration variables for shaped-charge jets. Ballistic Research Laboratory, Report No. 1184.

Baudin, G., Serradeill, et al. (2010) Review of Jones-Wilkins-Lee equation of state. EPJ Web of Conferences 10:21-21.

Chao G., Qu Z.J., Wang J., Hu D., Zhang Y. (2023). Study on jet formation behavior and optimization of trunconical hypercumulation shaped charge structure. Defence Technology 21 (03): 196-206. .

Chen C. (2015). Research on Tandem Matching and Explosion Interrupter Mechanism of Full-caliber Shaped Charge. Ph.D. Thesis (in Chinese), Nanjing University of Science and Technology, China.

Chou P.C., Carleone J. (1997). The Stability of Shaped Charge Jets. Journal of Applied Physics 48(10):4187-4195.

Chou P.C., Grudza M., Liu Y. F., et al. (1992). Shaped charge jet breakup formula with metal anisotropy. Proceedings of the 13th International Symposium on Ballistics 1992: 489-496.

Elshenawy T., Elbeih A., Li Q.M. (2018). Influence of target strength on the penetration depth of shaped charge jets into RHA targets. International Journal of Mechanical Sciences 136:234-242.

Elshenawy T., Li Q.M. (2013). Influences of target strength and confinement on the penetration depth of an oil well perforator. International Journal of Impact Engineering 54(APR.):130-137.

Fang Y.Z., Zhang X.F., Xiong W., et al. (2023). Study on penetration law of shaped charge jet considering shape distribution characteristics. Transactions of Beijing Institute of Technology, 43(10):1047-1058.

Funston, R., Mattsson, K., Ouye, N. (2002). K-charge-a multipurpose shaped charge warhead. EP.

Grove B., Heiland J., Walton I. (2008). Geologic materials' response to shaped charge penetration. International Journal of Impact Engineering, 2008, 35(12):1563-1566.

Guo H G, Su C H, Cai Y Q, et al. (2023). Reactive jet density distribution effect on its penetration behavior. Defence Technology, 24: 190-202.

Held M., Kozhushko A.A. (1999). Radial Crater Growing Process in Different Materials with Shaped Charge Jets. Propellants, Explosive, Pyrotechnics 24(6):339-342.

Hong B.H., Li W.H., Li Y.M., et al. (2024). Jet formation and penetration performance of a double-layer charge liner with chemically-deposited tungsten as the inner liner. Defence Technology 33(03):374-385.

Li G., Cheng X.W. (2022). A compressible model of radial crater growth by shaped-charge jet penetration. Explosive and Shock Waves 42(7):9.

Li Q.M., Meng H. (2003). About the dynamic strength enhancement of concrete-like materials in a split Hopkinson pressure bar test. International Journal of Solids & Structures 40(2):343-360.

Manfred H. (1995). Verification of the equation for radial crater growth by shaped charge jet penetration. International Journal of Impact Engineering 17: 387—398.

Rosenberg Z., Dekel E. (1994). A critical examination of the modified Bernoulli equation using two-dimensional simulations of long rod penetrators. International Journal of Impact Engineering 15(5):711-720.

Schwartz W. (1994). Modified SDM Model for the Calculation of shaped charge hole profiles. Propellants, Explosives, Pyrotechnics 19:192.

Shi G., Huang Z., Zu X., et al. (2026). Theoretical and experimental investigation of shaped charge jet penetration in soil targets with varying moisture content. Granular Matter, 28(2).

Simon J., Dipersio R. (1964). The penetration-standoff relation for idealized shaped charge jets. Ballistic Research Laboratory Memorandum, Report 1542.

Simon J., Dipersio R., Merendino A.B. (1965). Penetration of shaped-charge jets into metallic targets. Ballistic Research Laboratory Memorandum, Report No. 1296.

Song P., Li W.B., et al. (2019). The constitutive behavior of Ti–5Al–3V–2Cr–2Fe under high-velocity impact: Experimental, modeling, and validation. Journal of Alloys and Compounds 811:151946.-

Szendrei T. (1983). Analytical model of crater formation by jet impact and its application to calculation of penetration curves and hole profiles. The Hague: Proceedings of the 7th International Symposium on Ballistics.

Walters W.P., Flis W.J., Chou P. C. (1988). A survey of shaped-charge jet penetration models. International Journal of Impact Engineering 7(3):307-325.

Wang Z.Z. (2006). The destroy mechanism study of plate structure under shaped charge. Harbin Engineering University, China.

Wang J., Wang C., Ning J.G. (2008). Theoretical model for the calculation of concrete target resistance and numerical simulation of penetration by shaped charge jets. Acta Armamentarii 29(12):1409-1416.

Wang J., Wang C., Ning J.G. (2009). Theoretical model for shaped charge jets penetration and cavity radius calculation. Engineering Mechanics 26(4): 1-26.

Wang F., Jiang J.W., Men J. B. (2018). A Penetration Model for Tunsgsten-copper Shaped Charge Jet with Non-constant Density. Acta Armamentarii 39(12):9.

Wang Y., Li W., Zhu G., et al. (2019). Oblique Penetration of a Circular Pipe Target by a Prefabricated Fragment. International Journal of Structural Stability and Dynamics. https://dx.doi.org/10.1142/S0219455419501190.

Wright T.W., Frank K. (1988). Approaches to Penetration Problems. Ballistics Research Laboratory.

Xiao Q.Q., Huang Z.X., Gu X.H. (2010). Engineering Research on Radial Crater Growth for the Penetration in Concrete Target by Shaped Charge Jet. Acta Armamentarii (4):5.

Xiao Q.Q., Huang Z.X., Gu X.H. (2011). Equation of Penetration and Crater Growth by Shaped Charge Jet under the Influence of Shock Wave. Chinese Journal of High Pressure Physics 25(04):333-338.

Xiao Q.Q., Huang Z.X., Zu X.D., et al. (2020). Shaped charge penetration into high-and ultrahigh-strength Steel-Fiber reactive powder concrete targets. Defence Technology 16(01):217-224.

Xiao Q.Q., Huang Z.X., Zu X.D., et al. (2026). The effects of compressibility and target strength on shaped charge jet penetration. Defence Technology, 56.

Xu W.L., Wang C., Chen D.P. (2019). The jet formation and penetration capability of hypervelocity shaped charges. International Journal of Impact Engineering 132(OCT.): 103337.1-103337.15.

Yang L., Chen C., Zhang J., et al. (2016). Analysis of Formation Experiment and Penetration Property of Rod-like Jet of Shaped Charge with Foam. Acta Armamentarii, 37(4): 621-626.

Zhao L.J., Hao Y.P., Huang X.J. (2023) Numerical simulation and experimental research on jetting projectile charge penetrating 45 steel target. Journal of Ordnance Equipment Engineering, 44(8): 147-153.